Rev. LatinAm. Metal. Mat.

Artículo Regular

www.rlmm.org

PHASE DIAGRAM OF $(CuInTe_2)_{1-x}$ $(FeTe)_x$ ALLOYS $(0 \leq x \leq 0.6)$

P. Grima-Gallardo[1,], M. Quintero[1], L. Nieves[1], H. Cabrera[2, 3], E. Perez-Cappe[4], I. Zumeta-Dubé[5], J.A. Aitken[6] and J.A. Brant[6]*

1: Centro de Estudios en Semiconductores (CES). Departamento de Física. Facultad de Ciencias. Universidad de Los Andes (ULA). Mérida. Venezuela. 2: SPIE-ICTP Anchor Research in Optics Laboratory, International Centre for Theoretical Physics (ICTP), Strada Costiera 11, Trieste, Italy. 3: Centro Multidisciplinario de Ciencias, Instituto Venezolano de Investigaciones Científicas (IVIC), 5101 Mérida, Venezuela. 4: Instituto de Ciencia y Tecnología de Materiales (IMRE), Universidad de La Habana, Vedado, Cuba. 5: Instituto Politécnico Nacional, Centro de Investigación en Ciencia Aplicada y Tecnología Avanzada, Unidad Legaria, 11500 México D.F, México. 6: Department of Chemistry and Biochemistry, Duquesne University, Pittsburgh, USA.

**e-mail: peg@ula.ve (P. Grima-Gallardo)*

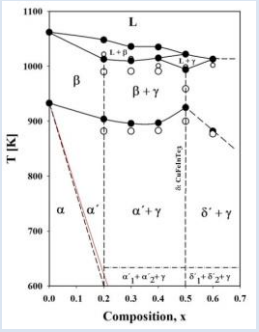

ABSTRACT

Polycrystalline samples of the (CuInTe2)1-x (FeTe)x alloy system where prepared by the melt and anneal technique and the products characterized by X-Ray Diffraction (XRD), Differential Thermal Analysis (DTA) and Optical Diffuse Reflectance Spectroscopy (ODRS) techniques. A first sight, samples were composed by a tetragonal phase with traces of a secondary phase identified as Fe1.125Te. Under exhaustive examination, it was found that the tetragonal phase, at the same time, is composed by two phases, with the same crystal structure and close lattice parameters, typical of spinodal decomposition. From ODRS measurements, optical absorption vs energy curves was obtained. These curves show how the addition of Fe produces a disordering-reordering process in the cationic sublattice suggesting that composition x=0.5 (CuFeInTe3) could be an intermediate compound in the diagram. Using the obtained information, a preliminary T-x phase diagram is proposed.

Keywords: $CuInTe_2$, FeTe, solid solutions, X-Ray Diffraction, Differential Thermal Analysis, Optical Diffuse Reflectance Spectroscopy, T-x Phase Diagram.

DIAGRAMA DE FASES DEL SISTEMA DE ALEACIONES $(CuInTe_2)_{1-x}$ $(FeTe)_x$ $(0 \leq x \leq 0.6)$

RESUMEN

Se prepararon muestras policristalinas del sistema de aleaciones (CuInTe2)1-x (FeTe)x por la técnica de fusión y recocido; los productos fueron caracterizados por las técnicas de Difracción de Rayos X (DRX), Análisis Térmico Diferencial (ATD) y Reflectancia por Espectroscopía de Óptica Difusa (REOD). A primera vista, las muestras se componen de una fase tetragonal con trazas de una fase secundaria identificada como Fe1.125Te. Bajo un examen más exhaustivo, se encontró que la fase tetragonal se compone a su vez de dos fases, con la misma estructura cristalina y parámetros de red cercanos, típico de una descomposición espinodal. A partir de mediciones REOD, se obtuvieron las curvas de absorción óptica vs energía. Estas curvas muestran cómo la adición de Fe produce un proceso de desorden-reorden en la subred catiónica que sugiere que la composición x = 0,5 (CuFeInTe3) podría ser un compuesto intermediario en el diagrama. Con la información obtenida, se propone un diagrama de fases T-x.

Palabras Claves: $CuInTe_2$, FeTe, soluciones sólidas, Difracción de Rayos-X, Análisis Térmico Diferencial, Reflectancia por Espectroscopía de Óptica Difusa, Diagrama de fases T-x.

Recibido: 31-10-2016 ; **Revisado:** 22-04-2017

Aceptado: 29-06-2017 ; **Publicado:** 20-08-2017

pISSN: 0255-6952 | eISSN: 2244-7113

Rev. LatinAm. Metal. Mat. 2018; **38** (1): 53-63

1. INTRODUCTION

$CuInTe_2$ (CIT) is a well-known semiconductor belonging to the ternary chalcopyrite I-III-VI_2 family that crystallizes in the tetragonal structure s. g. ($I\bar{4}2d$) with lattice parameters a=6.184 Å and c=12.37 Å (c/a=2.000) [1-2]. It melts congruently at 1062K and shows a solid-to-solid phase transition (from chalcopyrite to sphalerite structure) at 945K [3]. The optical energy gap (E_g) has been measured in the temperature range 300 to 550K, obtaining a linear variation of E_g with T given by the expression: E_g [eV/K]($T_{300\text{-}550}$) = 0.94 – 0.00053T [4]. As-growth samples show always p-type conduction [5] although under particular conditions it can be changed to n-type [6].

From the point of view of their technological applications, CIT has been indicated as a promising material for thermoelectric conversion since their zT value reaches 1.18 at 850 K, better than any other un-doped diamond-like material [7]. Also, it has been investigated for photovoltaic applications, however only relative low efficiencies are observed until now: ~4% [8-9] and ~7% [10], compared with the analogous chalcopyrite $Cu(In,Ga)Se_2$ material for which efficiencies as high as 21.7% has been recently measured [11].

Several alloy families of the type $(CuInTe_2)_{1-x}$(II-Te)$_x$ (II: metal transition) have been investigated (see Table I). It can be observed that the chalcopyrite single phase field exists only in the composition range x<0.3 in all the cases showed in Table II. This result is in agreement with theoretical calculations using the VanVechten's suggestion [18] that the difference in the band gap between the ordered chalcopyrite and the disordered zinc-blende phase is expected to be proportional to the extrinsic bowing parameter (see eq. 2 below).

With respect to $(CuInTe_2)_{1-x}(FeTe)_x$ alloys, only x=0.5 composition has been reported [6]. X-ray power diffraction indicates that this sample is composed by a tetragonal chalcopyrite-like phase with lattice parameters very close to CIT and traces of a secondary phase identified as $Fe_{1.125}Te$. It was also reported that addition of Fe to $CuInTe_2$ changes the electrical conductivity from *p*-type to *n*-type and decrease the thermal conductivity giving an increase in the *zT* figure of merit with respect to pure CIT.

In this work we are investigated the $(CuInTe_2)_{1-x}(FeTe)_x$ alloy system in the composition range $0 \leq x \leq 0.6$ and proposed a preliminary phase diagram.

Table I. Summary of experimental work on $(CuInTe_2)_{1-x}$(II-Te)$_x$ alloys (II: metal transition).

Transition metal II	single chalcopyrite phase field (α)	Remarks	References
Zn	$0 \leq x < 0.3$	Two-phases (α+β) for $0.3 \leq x \leq 0.4$ Single disordered sphalerite β-phase for $0.4 < x \leq 1$	[12-13]
Cd	$0 < x < 0.2$	Single disordered sphalerite β-phase for $0.2 \leq x \leq 1$	[14-15]
Mn	$0 < x < 0.27$	Single disordered sphalerite β-phase for $0.27 \leq x \leq 0.55$	[16]
Hg	$0 < x < 0.27$	Single disordered sphalerite β-phase for $0.27 \leq x \leq 1$	[17]

Note: All the phase fields measured at 300K.

2. EXPERIMENTAL PROCEDURE

2.1 Preparation of the samples

Polycrystalline $(CuInTe_2)_{1-x}$ $(FeTe)_x$ samples were synthesized using the usual melt and anneal technique. The manner in which the samples have been prepared in this work, using the $(CuInTe_2)_{1-x}$ $(FeTe)_x$ stoichiometric equation, implies that Fe atoms occupy Cu and/or In crystallographic sites randomly. Stoichiometric quantities of Cu, Fe, In and Te elements with purity of 99.99% were charged in an evacuated synthetic silica glass ampoule, which was previously subjected to pyrolysis in order to avoid reaction of the starting materials with silica glass. Then, the ampoule was sealed under vacuum (~10^{-3} Torr) and the fusion

process was carried out inside a furnace (vertical position) heated up to 1500 K at a rate of 20 K/h, with a stop of 48 h at 722.5 K (melting temperature of Te) in order to maximize the formation of binary species at low temperature and minimize the presence of unreacted Te at high temperatures. The ampoule was shaken by a mechanical system during the entire heating process in order to help completely mix all the elements. When the maximum temperature (1500 K) was achieved, the ampoule was shaken for another 48 h before cooling at a rate of 20 K/h, until the temperature reached 873 K. The ampoule was kept at this temperature for a period of 30 days. Finally, it was cooled to room temperature at a rate of 10 K/h. The color of obtained ingots was bright gray and homogeneous in aspect.

2.2 X-Ray Powder Diffraction (XRD)

A small amount of the sample was thoroughly ground using an agate mortar and pestle and deposited on a zero-background specimen holder. X-ray powder diffraction patterns of the samples were recorded using a PANalytical X'Pert Pro MPD powder Xray diffractometer operating in Bragg-Brentano geometry using CuK_a radiation with an average wavelength of 1.54187 Å. A tube power of 45 kV and 40 mA was employed. A nickel filter was used in the diffracted beam optics and the data were collected by the X'Celerator one-dimensional silicon strip detector. A ¼° divergent slit, a ½° antiscatter slit, and a 0.02 rad soller slit were set at both the incident and diffracted beams. The scan range was from 5 to 145° 2θ with a step size of 0.008° and a scan speed of 0.0106°/s.

2.3 Differential Thermal Analysis (DTA)

Phase transition temperatures were obtained from DTA measurements, performed in vacuum in the temperature range of 300-1500 K, using a Perkin-Elmer DTA-7. The instrument was calibrated by performing measurements with aluminum and gold as references. The charge was approximately 100-mg of powdered alloy. Both heating and cooling runs were carried out on each sample; the average rates of these runs were approximately 10 K/min. The uncertainty in these temperature determinations was about ±10 K. The temperature values of the thermal transitions were obtained, as usual, using the intercept of the base line with the beginning of the corresponding peak.

2.4 Optical Diffuse Reflectance Spectroscopy (ODRS)

The optical diffuse reflectance spectrum was obtained using a Varian Cary 5000 UV/VIS/NIR spectrometer equipped with a Harrick Praying Mantis diffuse reflectance accessory that uses elliptical mirrors. The sample was ground and placed into a sample holder to a depth of 3 mm. Barium sulfate (Fisher, 99.92%) was used as a 100% reflectance standard. Data were collected in the range of 2500 to 200 nm at a scan rate of 600 nm/min.

3. RESULTS AND DISCUSSION

In Figure 1, the experimental diffractions patterns for the $(CuInTe_2)_{1-x}$ $(FeTe)_x$ alloy system in the composition range $0.2 \leq x \leq 0.6$ are displayed. For $CuInTe_2$ ($x = 0$) the diffraction pattern has been calculated using PowerCell software [19]. A first sight, the experimental diffractions patterns are composed by two phases: a tetragonal chalcopyrite-like phase with lattice parameters very close to $CuInTe_2$ and a secondary phase identified as $Fe_{1.125}Te$ [20]. However, under a more closer inspection (see Figure 2), it can be observed that the tegragonal (α) phase is in reality decomposed in two phases ($\alpha_1 + \alpha_2$) with the same crystal structure and very close lattice parameters which is typical of an spinodal decomposition (SD), a mechanism producing a rapid unmixing of a solid phase in two coexisting phases. In SD, in contrast with the nucleation and growth process, where the initial formation of microscopic clusters involve a large free energy barrier, there is not thermodynamic barrier to the reaction inside the spinodal region and the decomposition is solely determined by a difussion process that produce a finely dispersed structure of two phases, in this case, one Fe-poor (α_1) an another Fe-rich (α_2).

In figure 3, the calculated (using DIVOL06 software) lattice paramers (a and c) of α_1 and α_2 phases are showed. The lattice parameters of α_1 phase (Fe-poor) are very close to $CuInTe_2$ whereas those of the α_2 phase are a little lower since the difference in covalent radii values [21] of Fe^{2+} (1.25 Å) and Cu^{+1} (1.38 Å) or In^{+3} (1.44 Å). It is also observed that the parameter a varies very little with composition whereas the parameter c shows a appreciable positive linear variation.

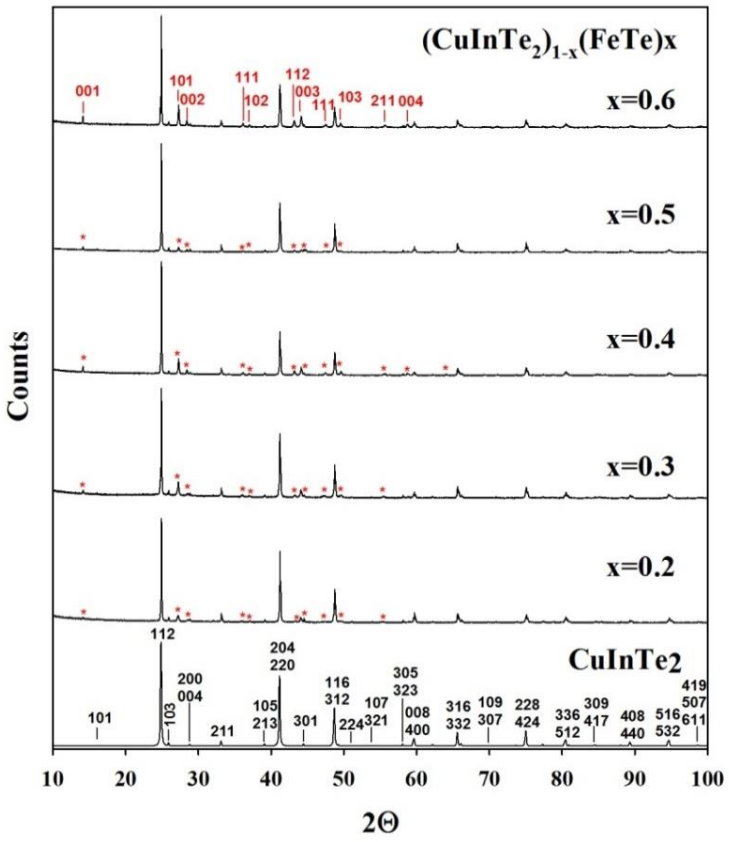

Figure 1. XRD patterns for the $(CuInTe_2)_{1-x}$ $(FeTe)_x$ alloy system. For $CuInTe_2$ (x = 0) the diffraction pattern has been calculated using PowerCell software [19]. Labels over the diffraction peaks correspond to the hkl-Miller indices (at the bottom in black: $CuInTe_2$; at the top in red: $Fe_{1.125}Te$). Asterisks identify the diffraction peaks positions of the $Fe_{1.125}Te$ secondary phase.

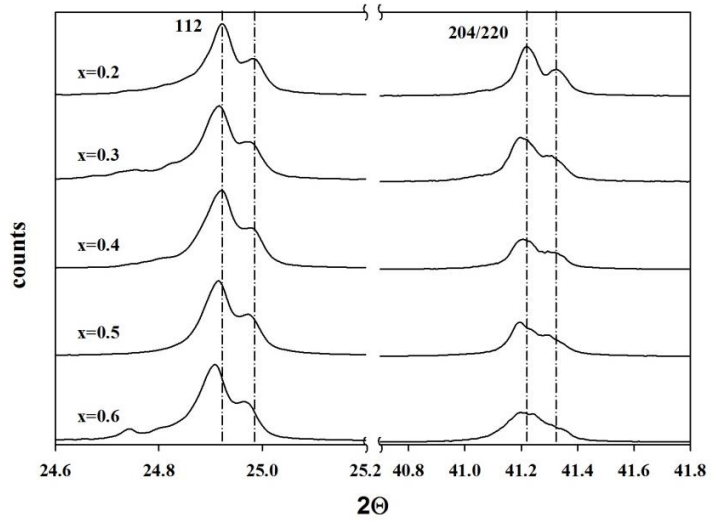

Figure 2. Spinodal decomposition in the (CuInTe2)1-x (FeTe)x alloy system. The figure shows the split of the strongest diffraction peaks of the tetragonal phase (112 and 204/220). The dash-dotted lines are a guide to the eye for best observation of the shift with composition.

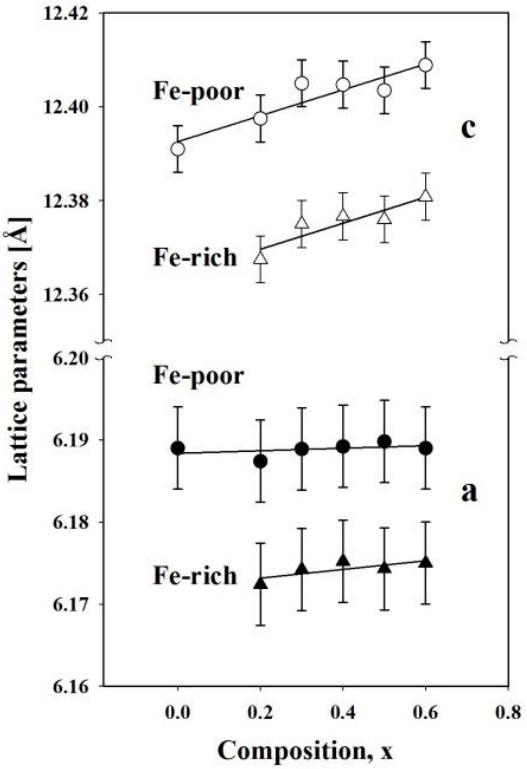

Figure 3. Lattice parameters vs composition for the tetragonal phase in the $(CuInTe_2)_{1-x}$ $(FeTe)_x$ alloy system: a (bottom, black circles Fe-poor phase; black triangles Fe-rich phase) and c (top, white circles Fe-poor phase; white triangles Fe-rich phase).

With respect to the $Fe_{1.125}Te$ secondary phase, it is sometimes referred to as β-FeTe (or more precisely $FeTe_x$, where *x* is less than unity), because the phase occurs at off-stoichiometric compositions. The β−phase is the Fe-richest intermediate phase, with a homogenety range close to "FeTe", which may have been a two-phase alloy [22]. It is worth to note here that the relative amount of the $Fe_{1.125}Te$ secondary phase with respect to the mean tetragonal phase, calculated from the relative intensities of their strongest diffraction peaks, does not increase monotonically with x as it is usual in alloys, showing a local minimum at x=0.5 (see figure 4). This behavior suggests that a reordering of the cationic sublattice take place at x = 0.5 with an increase of the solubility of Fein the ternary matrix. In a previous work, investigating the parent $(CuInSe_2)_{1-x}$ $(FeSe)_x$ solid solution system [23] it was proposed a crystallographic evolution with the incorporation of Fe, based in an order-disorder mechanism in the cationic sublattice, from the ordered chalcopyrite (α-phase), space group $I\bar{4}2d$ at x = 0 to a semi-ordered chalcopyrite-like phase (α´-phase), space group $P\bar{4}2c$ in the interval 0 < x < 2/3 to a re-ordered stannite phase (δ-phase), space group $I\bar{4}2m$ at x = 2/3.

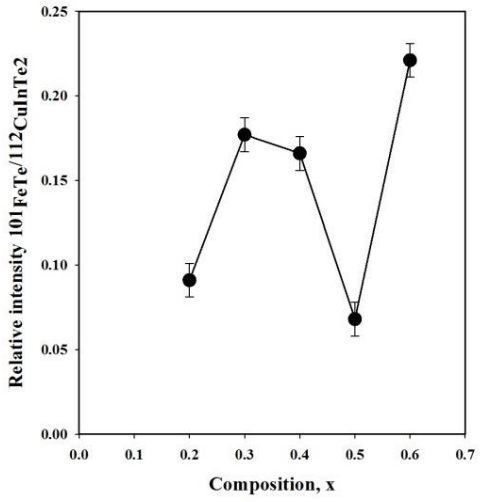

Figure 4. Relative intensity of the strongest diffraction lines 101 ($Fe_{1.125}Te$) and 112 ($CuInTe_2$). The solid line is only a guide to the eyes.

Rietveld refinement analysis of $CuFeInSe_3$ [24], $CuTaInTe_3$ [25], $CuFeAlSe_3$ and $CuFeGaSe_3$ [26], $CuNiGaSe_3$ and $CuNiInSe_3$ [27] in the space group $P\bar{4}2c$ and also $CuTa_2InTe_4$ [28], $CuFe_2InSe_4$ [29] $AgFe_2GaTe_4$ [30] $CuFe_2AlSe_4$ and $CuFe_2GaSe_4$ [31] in $I\bar{4}2m$ holds the former hypothesis. Please note than in the $(I\text{-}III\text{-}VI_2)_{1-x}(MT\text{-}VI)_x$ nomenclature, the compositions x = 0.5 and x = 2/3 can be written as $I\text{-}MT\text{-}III\text{-}VI_3$ and $I\text{-}MT_2\text{-}III\text{-}VI_4$, respectively.

In figures 5, the DTA heating and cooling cycles are given. There are two or three peaks clearly visible for each composition in both cycles. The peak at the lower temperature can be attributed, in analogy with $CuInTe_2$, with an order-disorder phase transition, whereas the other(s) correspond to the melting (solidification) process which is incongruent (solid → solid + liquid → liquid) with the exception of *x* = 0.6 composition.

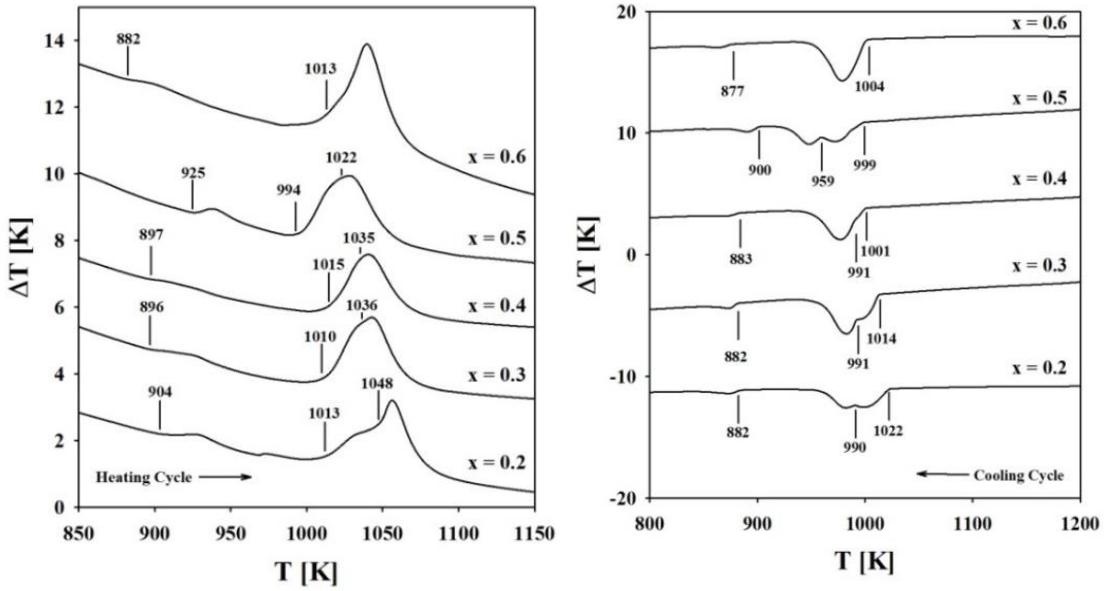

Figure 5. DTA heating (left side) and cooling (right side) cycles for the $(CuInTe_2)_{1-x}$ $(FeTe)_x$ alloy system.

The order-disorder transition temperature is also noted as T_c in literature. The dependence of the T_c with composition can be roughly calculated using an extension of the Van Vechten theory [18, 32-34]:

$$T_c = (\beta \Delta E_g + T_0^{0.5})^2 \quad (1)$$

$\beta = 43.941\ K^{0.5}eV^{-1}$ and $T_0 = 132.64K$ are constants obtained from the fit of experimental values [33] and ΔE_g is the variation of the band gap between ordered and disordered phases given by:

$$\Delta Eg = \alpha_{AB} C^2 / A_0 \quad (2)$$

$A_0 \approx 1$ eV is the effective band width parameter, α_{AB} is a correction factor which depends of the involved cations (for Cu and In is 0.040) and C is defined as:

$$C = 1.5e^2 (Z_B / r_B - Z_A / r_A) \exp(-kR) \quad (3)$$

A and B denotes the constituent cations of the ternary ABC_2, e is the electron charge, Z represents the valence number of cations, r the covalent radii, $k = (4.045x\ 10^4/a^{0.5})\ cm^{-1}$ is the screening wave number related with the lattice parameter (a) of the ternary and $R = (r_A+r_B+2r_C)/4$ is the arithmetic average of r.

The dependence with composition is obtained using:

$$r_A(x) = r_A(1-x) + r_D(x) \quad (4)$$

$$r_B(x) = r_B(1-x) + r_D(x) \quad (5)$$

$$\alpha_{AB}(x) = \alpha_{AB}(1-x^2) \quad (6)$$

The label D identifies the substitute cation in the alloys, Fe in this work. In our calculation we are

used r_{Cu}=1.38Å, r_{In}=1.44 Å, r_{Te}=1.35 Å y r_{Fe}=1.25 Å [21] and a=6.179 Å [1-2]. The parameter A_0 has been taken as 0.89 eV so that the calculated value of the order-disorder transition temperature matches with experimental [34].

Figure 6 shows the diffuse reflectance spectra of the $(CuInTe_2)_{1-x}$ $(FeTe)_x$ powder samples with $0.2 \leq x \leq 0.6$ measured by UV-vis-NIR spectroscopy. Figure 7 shows an $[F(R)h\nu]^2$ vs hν plot of the diffuse reflectance spectra of powders with compositions *x* = 0,2, 0.3, 0.4, 0.5 y 0.6 (from left to right, respectively). F(R) denotes the Kubleca-Mulk function of the reflectance spectra.

In figure 7, it is observed that substitution of Cu/In cations with Fe, induces an increase in the absorption intensity i.e the absorption increase with the x value. The absorption spectra, in the energy interval 0.5 to 6 eV, is composed by a strong peak at ~ 1 eV which corresponds to a direct transition along the Γ–Γ point (E_g) and another very broad peak centered at ~ 3 eV due to direct transitions along L-L and X-X points [36].

The function F(R) is also called the absorbance A_b and it is proportional to the absorption coefficient α. The optical energy gap E_g is obtained based in the following equation:

$$\alpha h\nu = A\left(h\nu - E_g\right)^n \qquad (7)$$

Where the parameters A and n are constants, and ν is the photon frequency of the incident light. The parameter A depends of the temperature and photon energy [35] and the values of the exponent n should be 1/2 for direct transitions or 2 for indirect. The optical band gaps were determined by extrapolating the linear portion of the curve to the *X* axis, the cross point in the *X* axis correspond to E_g. The E_g band-gap values have been plotted vs composition in figure 8.

Figure 8, is very illustrative of the previous comment about disorder of the cation sublattice. When the sample is highly disordered a broad shoulder appears centered at ~ 0.8 eV (see x = 0.3) whereas for a quasi-ordered sample (x = 0.5), this shoulder almost disappears. The behavior of E_g given in figure 8 is completely coherent with figure 4: E_g decreases in the interval $0 \leq x \leq 0.3$, increases for $0.4 \leq x \leq 0.5$ and then decreases again for x = 0.6.

Using all the information obtained, a preliminary T-x phase diagram is proposed in figure 9.

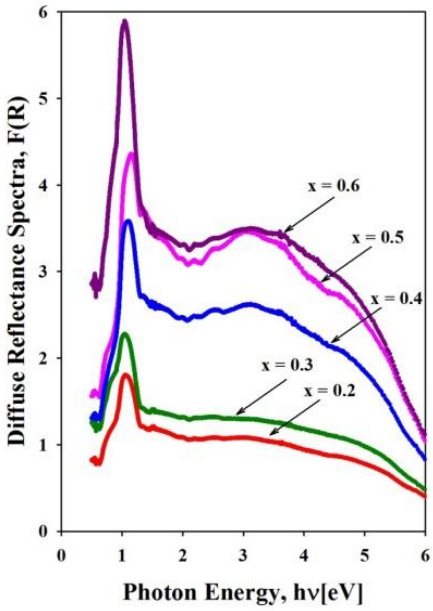

Figure 6. Diffuse reflectance spectra of $(CuInTe_2)_{1-x}$ $(FeTe)_x$ samples with $0.2 \leq x \leq 0.6$ measured by UV-vis-NIR spectroscopy.

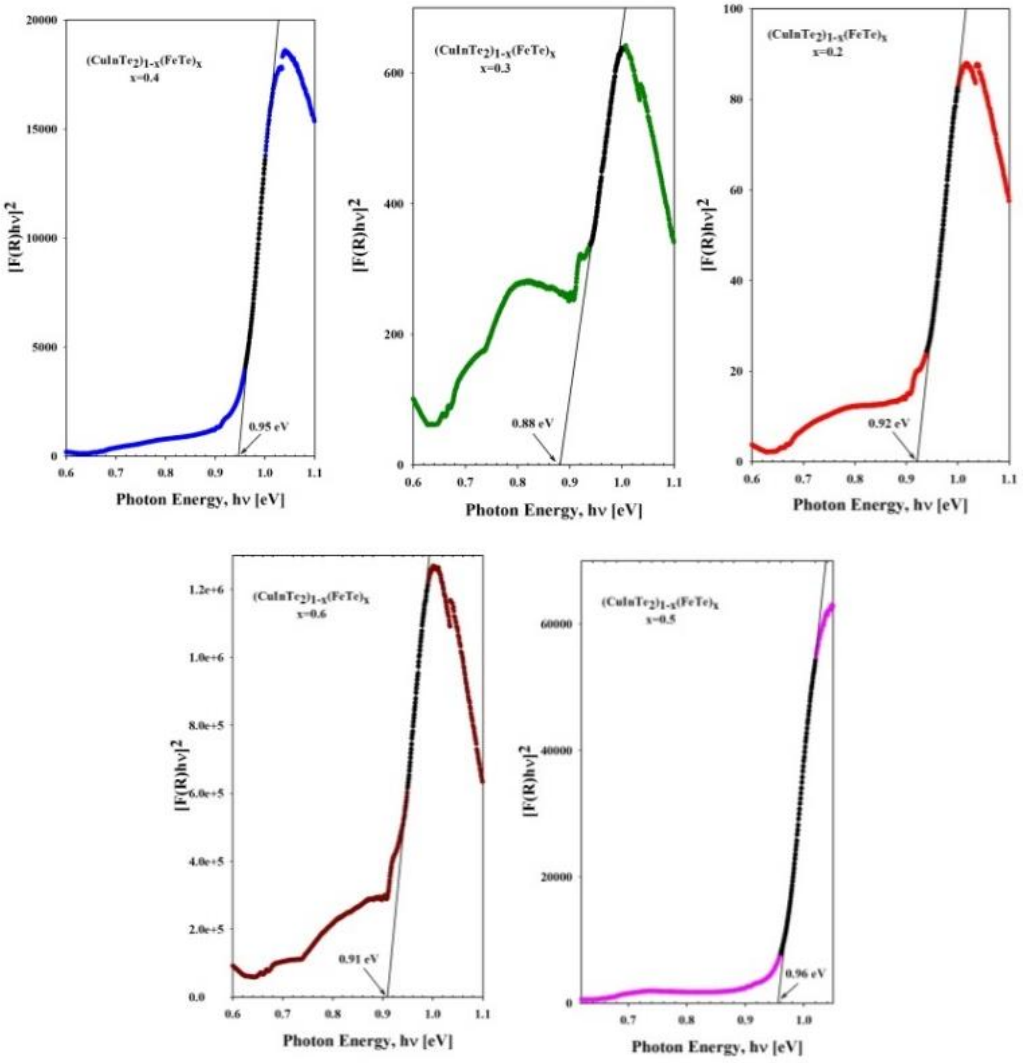

Figure 7. Plots of $[F(R)h\nu]^2$ *vs* $h\nu$ for x = 0.2, 0.3, 0.4, 0.5 and 0.6 compositions (from left to right, respectively). The solid line is a fit on the linear part (black circles) of the curve.

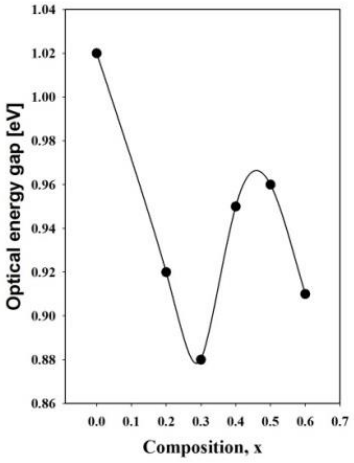

Figure 8. Band-gap energies of $(CuInTe_2)_{1-x}(FeTe)_x$ estimated from the $[F(R)h\nu]^2$ vs hν plot of the reflectance spectra. The line is only a guide for the eyes.

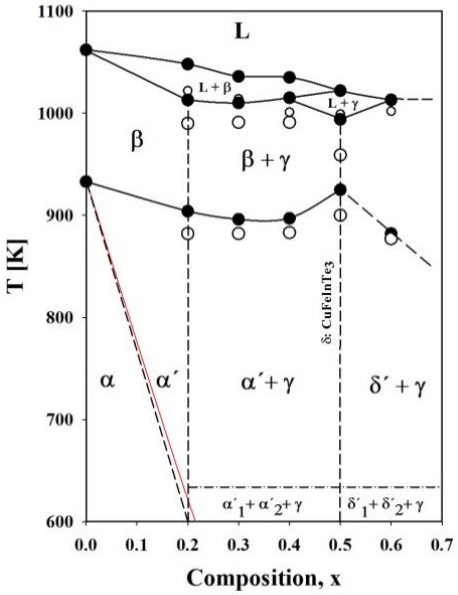

Figure 9. T vs x phase diagram for $(CuInTe_2)_{1-x}(FeTe)_x$ alloy system. Heating cycle: black circles. Cooling cycle: white circles. Dashed lines and dashed-dotted lines: proposed field boundaries. Red line: Van Vechten's model. α: Ordered chalcopyrite; α´: semi-ordered-chalcopyrite; α_1: Fe-poor semi-ordered chalcopyrite; α_2: Fe-rich semi-ordered chalcopyrite; β: disordered sphalerite; δ: ordered stannite; δ´: semi-ordered stannite; γ: $Fe_{1.125}Te$; L: liquid.

At 600K (the annealing temperature) the chalcopyrite (α) single phase field extends in the composition range $0 \leq x < 0.2$. In the interval $0.2 \leq x < 0.5$ three phases were observed: α'_1 (Fe-poor semi-ordered-chalcopyrite), α'_2 (Fe-rich semi-ordered-chalcopyrite) and γ ($Fe_{1.125}Te$) whereas for the interval $0.5 \leq x \leq 0.6$, the α'_1 and α'_2 phases converts in δ'_1 and δ'_2. At x=0 ($CuInTe_2$) the chalcopyrite α-phase transforms into the sphalerite β-phase at 933K [21]. The boundary between α and α´ phases is showed as a dashed line which almost coincides with Van Vechten´s model (red line). The boundary where the spinodal decomposition occurs is signaled as a dashed-dotted line at a relative arbitrary temperature since no peaks are observed in DTA thermograms indicative that the energy associated to this transition is very low. The boundaries corresponding to $\alpha' \rightarrow \alpha'+\gamma \rightarrow \delta'+\gamma$ phase fields are signaled by vertical dashed lines at x=0.2 and x=0.5, respectively. The β-phase field extends from 933 to 1060K at x=0 and from 905 to 1014K at x=0.2 whereas the β+γ field extends from 905 to 1014K at x=0.2 and from 925 to 995K at x=0.5. Relative narrows L+β and L+γ fields separate the solid and liquid (L) phases in the interval $0 \leq x \leq 0.6$.

4. CONCLUSIONS

$(CuInTe_2)_{1-x}(FeTe)_x$ solid solutions in the composition interval $0 \leq x \leq 0.6$ has been investigated. It was found that these samples are composed by a tetragonal chalcopyrite-like α-phase accompanied by traces of a $Fe_{1.125}Te$ secondary γ-phase. The amount of this secondary γ-phase do not increase monotonically with composition, but increases for $0.2 \leq x \leq 0.3$, then *decreases* for $0.4 \leq x \leq 0.5$ and finally increases again for $x = 0.6$. Also, the tetragonal α-phase undergoes to a spinodal decomposition which transform the original a-phase in two (α_1 and α_2) phases with the same crystal structure and very close lattice parameters. From optical absorption measurements, the band gap has been obtained as a function of composition. The shape of the optical absorption and values of the band-gap inversely follows the behavior of the amount of the secondary phase: decreases for $0.2 \leq x \leq 0.3$, increases for $0.4 \leq x \leq 0.5$ and decreases for x=0.6, suggesting that the amount of secondary phase modules E_g bias the disorder of the cationic sublattice. With these results a preliminary T-x phase diagram has been proposed.

With respect to the possible applications of these alloys, spinodal alloy decomposition (chemical

phase separation) into regions incorporating either very large or very small concentration of the magnetic constituent and disorder-driven electronic phase separation into ferromagnetic bubbles containing a large carrier density immersed in a deplected paramagnetic environment, give place to superparamagnetic behavior or room temperature ferromagnetism, two characteristics of spintronics devices.

5. ACKNOWLEDGEMENT

P.G-G wants to thank to CDCHTA-ULA grant code C-1885-14-05-B and Fondo Nacional de Ciencia, Tecnología e Innovación (FONACIT) project number 2011001341. I.Z-D acknowledges postdoctoral fellow from CONACyT project number 174247 (Desarrollo de Materiales para Tecnologías de Energías Renovables).

6. REFERENCES

[1]. Shay J. L. and Wernick J. H., Ternary Chalcopyrite Semiconductors: Growth, Electronic Properties, and Applications (Pergamon Press, Oxford, 1975).

[2]. Bodnar I.V., Viktorov I.A. and Zabelina I.A. Russian J. Inorg. Chem., 1993; 38: 809-813.

[3]. Palatnik L.S. and Rogacheva E.I. Sov. Phys. Dokl 1967; 12: 503.

[4]. C. Power, P. Grima-Gallardo, M. Muñoz and I. Molina. Rev. LatinAm. Metal. Mat. 2011; 31(2): 134-137.

[5]. Zhang S.B., Wei S.-H. and Zunger A. J. Appl. Phys. 1998; 83(6); 3192-3196.

[6]. Cabrera H., Zumeta-Dubé I., Korte D., Grima-Gallardo P., Alvarado F., Aitken J.A., Brant J.A., Zhang J.H., Calderón A., Marín E., Aguilar-Frutis M., Erazo J.E., Perez-Cappe E., Franko M. J. Alloys and Compounds 2015; 651:490-496.

[7]. Liu R., Xi L., Liu H., Shi X., Zhang W. and Chen L. Chem Commun. 2012; 48(32): 3818-3820.

[8]. Lakhe M. and Chaure N.B. Solar Energy Materials and Solar Cells 2014; 123: 122-129.

[9]. Lakhe M., Mahapatra S.K. and Chaure N.B. Materials Science and Engineering: B 2016; 204: 20-26.

[10]. Mise T. and Nakada T. Prog. Photovolt: Res. Appl. 2013; 21:754–759.

[11]. Jackson P., Hariscos D., Wuerz R., Kiowski O., Bauer A., Friedlmeier T.M. and Powalla M. Phys. Stat. Sol. RRL 2015; 9(1): 28-31.

[12]. Bodnar I.V., Korzun B.V. and Chibusova L.V. Phys. Stat. Sol. (a) 2000; 179: 305-309.

[13]. Tovar R., Quintero M., Neal Ch. and Woolley J.C. J. Crys. Growth 1990; 106: 629.

[14]. Chernyavskii V.P., Goryunova N.A and Borshchevkii. Chemical Bonds in Solids. Proceedings of the International Symposium on Chemical Bonds in Semiconducting Crystals, held in Minsk, USSR, 1967. Vol. 4: Semiconductor Crystals, Glasses and Liquids. Edited by N.N. Sirota. Consultant Bureau. New York-London 1972.

[15]. Quintero M., Guerrero E., Tovar R. and Pérez G.S. J. Solid State Chem. 1990; 87: 456.

[16]. Quintero M., Grima P., Tovar R., Pérez G.S. and Woolley J.C. Phys. Stat. Sol. (a) 1988; 107: 205-211.

[17]. Grima P., Quintero M. and Woolley J.C. J. Crys. Growth 1992; 119: 381-390.

[18]. J.A. Van Vechten, in Ternary and Multinary Compounds, edited by S.K. Deb and A. Zunger (Materials Research Society, Pittsburgh, 1987) p. 423.

[19]. Kraus W. and Nolze G. J. Appl. Cryst. 1996; 29:301-303.

[20]. Fruchart D., Convert P., Wolfers P., Madar R., Sénateur J.P. and Fruchart P. Mater. Res. Bull. 1975; 10:169-174.

[21]. www.periodictable.com/Properties/A/CovalentRadius.html.

[22]. The Fe-Te (Iron-Tellurium) system by Okamoto H. (ASM International) and Tanner L.A. (Lawrence Livermore National Laboratory). Bulletin of Alloy Phase Diagrams. Vol. 11, No 4, 1990.

[23]. Grima-Gallardo P., Torres S., Quintero M., Nieves L., Moreno E. and Delgado G.E. J. Alloys and Compounds 2015; 630: 146-150.

[24]. Mora A.J., Delgado G.E. and Grima-Gallardo P. Phys. Stat. Sol. (a) 2007; 204:547.

[25]. Delgado G.E., Mora A.J., Grima-Gallardo P., Durán V., Muñoz M. and Quintero M. Cryst. Res. Technol. 2008; 43(7): 783–785.

[26]. Delgado G.E., Mora A.J., Contreras J.E., Grima-Gallardo P., Durán S., Muñoz M. and Quintero M. Cryst. Res. Technol. 2009; 44:548-552.

[27]. Delgado G.E., Mora A.J., Grima-Gallardo P., Durán S., Muñoz M. and Quintero M. Bull. Mater. Sci. 2010; 33(5): 637–640.

[28]. Delgado G.E., Mora A.J., Grima-Gallardo P., Muñoz M., Duran S. and Quintero M. Physica B: Condensed Matter 2008; 403:3228.

[29]. Delgado G.E., Mora A.J., Grima-Gallardo P. and

Quintero M. J. Alloys and Compond. 2008; 454:306-309.

[30]. Delgado G.E., Quintero E., Tovar R., Grima-Gallardo P., Quintero M. J. Alloys and Compounds 2014; 613:143–145.

[31]. Delgado G.E., Grima-Gallardo P. and Quintero M. Revista Mexicana de Física 2016; 62:393-397.

[32]. Van Vechten J.A., Ternary and Multinary Compounds (Materials Research Society, 1987), p. 423.

[33]. Rincón C. Phys. Rev. B 1992; 45:12716.

[34]. Grima-Gallardo P. Phys. Stat. Sol. (a) 1992; 134:119.

[35]. Hankare P.P., Rathod K.C., Chate P.A., Jadhav A.V. and Mulla I.S. J. Alloys and Compounds 2010; 500:78.

[36]. Tototzintle-Huitle, H., Rodríguez J.A. and Baquero. R. Revista Mexicana de Fisica 2008; 54(1): 58–64.